J Mater Sci (2011) 46:2091–2096
DOI 10.1007/s10853-010-5043-x

Glass-forming ability and thermoplastic formability of a $Pd_{40}Ni_{40}Si_4P_{16}$ glassy alloy

N. Chen · H. A. Yang · A. Caron · P. C. Chen · Y. C. Lin · D. V. Louzguine-Luzgin · K. F. Yao · M. Esashi · A. Inoue

Received: 10 September 2010 / Accepted: 29 October 2010 / Published online: 11 November 2010

Abstract The glass-forming ability of a $Pd_{40}Ni_{40}Si_4P_{16}$ alloy has been investigated. This alloy exhibits a wide supercooled liquid region of 107 K, a high reduced glass transition temperature of 0.596 and a small fragility parameter of 28, indicating that this alloy is a good glass former. Using flux treatment, the $Pd_{40}Ni_{40}Si_4P_{16}$ alloys can be easily produced as centimeter-scale metallic glasses. The glass transition and crystallization kinetics of this alloy were investigated by means of both differential scanning calorimetry (DSC) and differential isothermal calorimetry (DIC). Thermoplastic forming of the $Pd_{40}Ni_{40}Si_4P_{16}$ glassy alloy is easily performed due to the high thermal stability and low viscosity of the supercooled liquid. By pressing a "flat" silicon wafer onto a sample within the thermoplastic forming region, the surface of the $Pd_{40}Ni_{40}Si_4P_{16}$ metallic glasses could be significantly smoothened. The final surface showed a reduced root mean square roughness R_q as low as $\sim$2 nm. This indicates a simple approach to prepare "flat" surfaces for metallic glasses.

N. Chen (✉) · H. A. Yang · A. Caron · P. C. Chen · Y. C. Lin · D. V. Louzguine-Luzgin · M. Esashi · A. Inoue
WPI Advanced Institute for Materials Research, Tohoku University, Sendai 980-8577, Japan
e-mail: chenn@wpi-aimr.tohoku.ac.jp

D. V. Louzguine-Luzgin · A. Inoue
Institute for Materials Research, Tohoku University, Sendai 980-8577, Japan

K. F. Yao
Department of Mechanical Engineering, Key laboratory for Advanced Materials Processing Technology, Tsinghua University, Beijing 100084, China

Introduction

Bulk metallic glasses (BMGs) have attracted lots of attention due to their outstanding mechanical, physical, and chemical properties and high potential in applications such as sporting goods materials, corrosion resistant materials, and machinery structural materials, etc. [1–4]. Very recently, the thermoplastic formability of metallic glasses has been highlighted and has opened new possibilities of fabricating micro- and nano-electromechanical devices (M/NEMS) [5–9]. Pd-based BMGs exhibit a larger supercooled liquid region (SLR) than most metallic glasses [5]; $Pd_{40}Ni_{40}P_{20}$ alloy has been extensively studied due to its high glass-forming ability (GFA) and high thermal stability [10–13]. Partially substituting Cu for Ni was found to further enhance the GFA as reported in a $Pd_{40}Ni_{10}Cu_{30}P_{20}$ metallic glass [14]. Using a similar approach of partially replacing P with Si, some of the authors reported on the development of quaternary $Pd_{40}Ni_{40}Si_xP_{20-x}$ glass formers [15]. Among the reported alloys, the $Pd_{40}Ni_{40}Si_4P_{16}$ alloy was found to exhibit the largest SLR. However, the GFA and further thermodynamic properties of this alloy have not been studied yet. In this study, we report on the formation of centimeter-scale $Pd_{40}Ni_{40}Si_4P_{16}$ BMGs. Given its large SLR, this alloy could be processed by thermoplastic forming (TF). For demonstration, the surface roughness R_q of the $Pd_{40}Ni_{40}Si_4P_{16}$ metallic glasses was significantly reduced through a replication of a "flat" silicon wafer with roughness of around 1 nm.

Experimental

Alloys with a nominal composition of $Pd_{40}Ni_{40}Si_4P_{16}$ (at.%) were prepared by melting the raw materials Pd, Ni,

P, and Si with high purity over 99.9 mass% in vacuumed fused silica tubes. Glassy ribbons with dimensions of ~12 mm in width and ~160 μm in thickness were prepared using a single-roller melt-spinner. Bulk samples with diameters up to 2 cm were produced by conventional copper casting and a combination of fluxing and water cooling. The structure of the as-prepared alloys was characterized by X-ray diffraction (XRD) with monochromatic Cu Kα radiation. The thermal stability of the samples was examined by differential scanning calorimetry (DSC). Differential isothermal calorimetry (DIC) was applied to investigate the devitrification of the specimens. The TF was performed using wafer bonder. The surface roughness was measured by atomic force microscopy.

Results and discussion

Figure 1 shows the XRD patterns of the as-prepared $Pd_{40}Ni_{40}Si_4P_{16}$ alloys with thickness up to 2 cm. Using fluxing technique, the $Pd_{40}Ni_{40}Si_4P_{16}$ alloys could be easily prepared as centimeter-scale BMGs. Using a conventional casting process, however, the critical diameter for fully glass formation is only 6 mm, much smaller than that of the glassy alloys prepared by flux treatment. When a conventionally cast rod with a diameter of 8 mm was examined by XRD, some sharp diffraction peaks appeared, corresponding to an orthorhombic Pd-rich phase as indicated in Fig. 1. The fluxing-induced enhancement of GFA is already known for Pd-based metallic glasses and arises from the suppression of heterogeneous nucleation [16].

The DSC traces of the as-cast $Pd_{40}Ni_{40}Si_4P_{16}$ alloy with diameter of 2 mm are shown in Fig. 2a. According to the criterion $\chi = (T_l - T_{sc})/(T_l - T_g)$ (T_l is the liquidus temperature upon heating, T_{sc} is the solidification temperature upon cooling, T_g is the glass transition temperature. Since $T_{sc} \geq T_g$, so $\chi \leq 1$) to evaluate the GFA of the present alloys [16, 17], the calculated χ values are 0.515 and 0.253 for the fluxed and as-cast samples, respectively. A larger χ indicates that a liquid can be undercooled more easily, which favors glass formation and also reflects a significant difference in the GFA of the unfluxed and fluxed $Pd_{40}Ni_{40}Si_4P_{16}$ alloys as shown in Fig. 1. With increasing heating rate, T_g, the initial crystallization temperature T_x and the peak temperature T_p all shift to higher temperature, displaying kinetic characteristics. Taking into account the dependence of T_g on heating rate, the activation energy for glass transition E_g is calculated to be 245 kJ/mol on the basis of the Kissinger's equation $\ln(T_g^2/\phi) = \ln(E_g/k_B K_0) + E_g/k_B T_g$ [18] (see the inset of Fig. 2a). In general Kissinger analysis has been derived for and applied to the peak temperature of phase transformation. However, as many

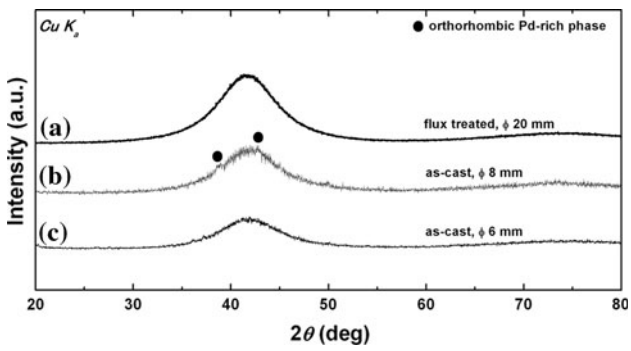

Fig. 1 XRD patterns of (*a*) the flux-treated $Pd_{40}Ni_{40}Si_4P_{16}$ alloy with a diameter of 20 mm and the cast $Pd_{40}Ni_{40}Si_4P_{16}$ alloys with diameters of (*b*) 8 mm and (*c*) 6 mm

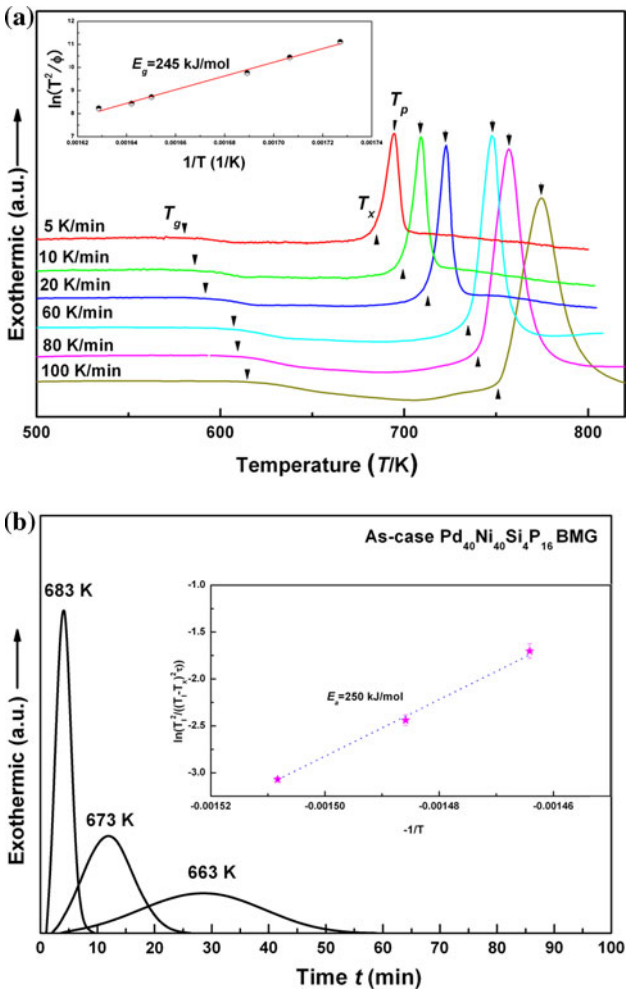

Fig. 2 **a** DSC curves of the $Pd_{40}Ni_{40}Si_4P_{16}$ bulk glassy alloys measured at different heating rate ranging from 5 to 100 K/min. The *inset* is the fitted Kissinger plot from which the activation energy for glass transition E_g was derived to be ~245 kJ/mol. **b** DIC curves of the $Pd_{40}Ni_{40}Si_4P_{16}$ bulk glassy alloys measured at temperatures of 683, 673, and 663 K, respectively. The *inset* is the plot of $\ln\left[(T_l)^2/\tau(T_l - T_x)^2\right]$ vs $(-1/T)$, yielding the activation energy ΔG_a for atomic diffusion of ~250 kJ/mol

Table 1 Thermodynamic, kinetic parameters, and derived parameters of the as-cast $Pd_{40}Ni_{40}Si_4P_{16}$ alloy

Heating rate (K/min)	T_g (K)	T_x (K)	ΔT (K)	T_m (K)	T_l (K)	T_{rg} (T_g/T_l)	γ ($T_x/(T_g + T_l)$)	m	E_g (kJ/mol)	ΔG_a (kJ/mol)
5	579	686	107	920	971	0.596	0.443	28	245	250
20	592	701	109	–						
40	609	728	119							

authors successfully applied this method to glass-transition phenomenon one can assume possible validity of this method for such a process, especially as near the glass-transition temperature the rate of changes in C_p attains the maximum. As listed in Table 1, the SLR ΔT (defined as $T_x - T_g$), the reduced glass transition temperature T_{rg} ($=T_g/T_l$) and γ ($=T_x/(T_g + T_l)$) of the $Pd_{40}Ni_{40}Si_4P_{16}$ alloy are derived based on the obtained kinetic and thermodynamic parameters. Compared with the $Pd_{40}Ni_{40}P_{20}$ alloy, the $Pd_{40}Ni_{40}Si_4P_{16}$ alloy shows larger ΔT and γ values [19], indicating that the $Pd_{40}Ni_{40}Si_4P_{16}$ alloy has better thermal stability and is more suitable for TF.

The fragility parameter m is another parameter to evaluate the GFA of the alloys, which is given by the following equation [20–22]:

$$m = (D^*/\ln 10) \times (T_g^0/T_g) \times (1 - T_g^0/T_g)^{-2} \quad (1)$$

where D^* is the strength parameter, T_g^0 is the asymptotic value of T_g and is usually approximated as the onset of glass transition at infinitely slow cooling. According to the concept of fragility, glass-forming liquids can be classified into three general categories: strong glass formers (<30), intermediate glass formers (30–100), and fragile glass formers (>100). Metallic glasses usually belong to the intermediate category in terms of their m values, normally ranging from 32 to 66 [23]. In general, for a smaller m, the GFA increases. As listed in Table 1, the fragility parameter m for the $Pd_{40}Ni_{40}Si_4P_{16}$ alloy is about 28, located in the range for strong glass formers.

Since the $Pd_{40}Ni_{40}Si_4P_{16}$ alloy shows a wide SLR, high thermoplastic formability of this alloy is expected. During the TF, a metallic glass is reheated into the SLR, where it turns into a metastable liquid. With increasing processing time the crystallization shall eventually set in, which would terminate the forming and destroy the fabricated parts. So a detailed understanding of the crystallization behavior of metallic glasses, particularly in the SLR, is needed.

The nucleation rate I_{ss} in the liquid is mainly governed by two exponential terms [24]. At high temperature the energy barrier for the formation of critical nuclei dominates, whereas the activation energy for atomic diffusion becomes overriding at low temperature. The TF temperatures lie in the SLR, which are very low with respect to the liquidus temperature of the alloy. Thus, during TF the dominant factor controlling the nucleation and subsequent crystallization is the kinetic barrier associated with the activation energy for atomic diffusion. The incorporation of the transient nucleation factor for the time-dependent nucleation rate, $I(t)$ is expressed by

$$I(t) = I_{ss} \exp(\frac{-\tau}{t}) \quad (2)$$

where the delay time, τ is given by

$$\tau = \frac{1}{\beta Z^2} = \frac{8k_B T\sigma a^4}{D\Delta G_V^2 C_s v_a^2} \quad (3)$$

In Eq. 3, v_a is the atomic vibration frequency in the liquid, σ is the interfacial energy, ΔG_V is the Gibbs free-energy difference, k_B is the Boltzmann constant, $D = a^2\upsilon\exp[-\Delta G_a/k_B T]$ is the diffusivity in the glass, where a describes the interatomic spacing. ΔG_a denotes the kinetic barrier corresponding to the activation energy for atomic diffusion in the glass and C_s is the solute concentration.

The delay time τ can provide an estimate of the controlling diffusivity. To determine the delay time, we performed the DIC measurement as shown in Fig. 2b, based on which τ was derived and was used to calculate the activation energy ΔG_a. We approximate ΔG_V by $\Delta H_f \cdot (T_l - T_x)/T_l$ where ΔH_f is the latent heat of fusion. Collecting the main temperature terms we obtain

$$\exp(-\frac{\Delta G_a}{k_B T})(\frac{T_l - T_x}{T_l})^2 = \frac{C}{\tau} \quad (4)$$

where C is a constant. Plotting $\ln\left[(T_l)^2/\tau(T_l - T_x)^2\right]$ vs $(-1/T)$ yields a straight line with a slope of $\Delta G_a/k_B$, as shown in the inset of Fig. 2b. We found $\Delta G_a = 250$ kJ/mol, which is very close to the activation energy for glass transition calculated with the Kissinger's equation.

The values of activation energies for the glass transition and atomic diffusion are close. In order to better understand these results, we consider the physics behind the glass-supercooled liquid transition and atomic diffusion. Both processes are kinetic in nature. The glass-supercooled liquid transition is controlled by kinetic factors, such as the viscosity. The activation energy for the glass transition is mainly ascribed to the increased internal energy associated with the reduced viscosity, and the work consumed for the volume expansion of the system. The latter can be

neglected due to the small structural difference in the glassy state as compare to the supercooled liquid frozen at the glass transition temperature [25, 26]. Accordingly the activation energy for glass transition is mainly used to enhance the atomic mobility, resulting in a decrease of the shear viscosity. On the other hand, it is supposed that the shear viscosity and the atomic diffusion are governed by the same relaxation processes of the free volume [27]. It means that the physical nature for both processes is a kinetic activation process for atomic motion, thereby yielding the close values of activation energies.

From the delay time for nucleation and crystallization determined by DIC curves, we set the TF temperature at 643 K, at which the delay time τ can reach $\sim$40 min, sufficiently long for TF process. Figure 3a shows the steps for molding with the $Pd_{40}Ni_{40}Si_4P_{16}$ metallic glassy ribbons. The TF is performed under a pressure of 80 MPa at 643 K as shown in Fig. 3b. Taking advantage of the low viscosity and favorable wetting properties of the supercooled liquid, the $Pd_{40}Ni_{40}Si_4P_{16}$ metallic glass has been fabricated into different structures as presented in Fig. 4. The structures shown in Fig. 4c and d were formed using the Si molds shown in Fig. 4a and b. Complicated structures could also be formed as shown in Fig. 4e and f, indicating that metallic glasses are good candidate materials for applications as MEMS. Figure 4g and h shows the porous alumina and the transferred nano-scale rods with diameters of $\sim$100 nm on the $Pd_{40}Ni_{40}Si_4P_{16}$ alloy, respectively.

Since metallic glasses are intrinsically exempted from a grain size limitation, theoretically the replicated feature size by the TF of metallic glasses can be as small as atomic-level [8, 9]. Now, we consider an extreme example of a mold with infinitesimal patterns, namely, a perfect flat surface. If the perfect flat surface is directly pressed onto metallic glasses during TF region, then the surface roughness of metallic glasses would correspond to the experimentally accessible minimum feature size. However, it is difficult to find such a perfect flat surface. Instead, we used a "flat" Si wafer with roughness of about 1 nm to test the above supposition. The original ribbon sample shows a root mean square (rms) surface roughness R_q of around 15 nm (Fig. 5a). After pressed by a "flat" silicon wafer, the ribbon surface becomes smoother with a reduced rms roughness R_q of about 9 nm as shown in Fig. 5b. A selected area shows a rms roughness R_q down to 2 nm

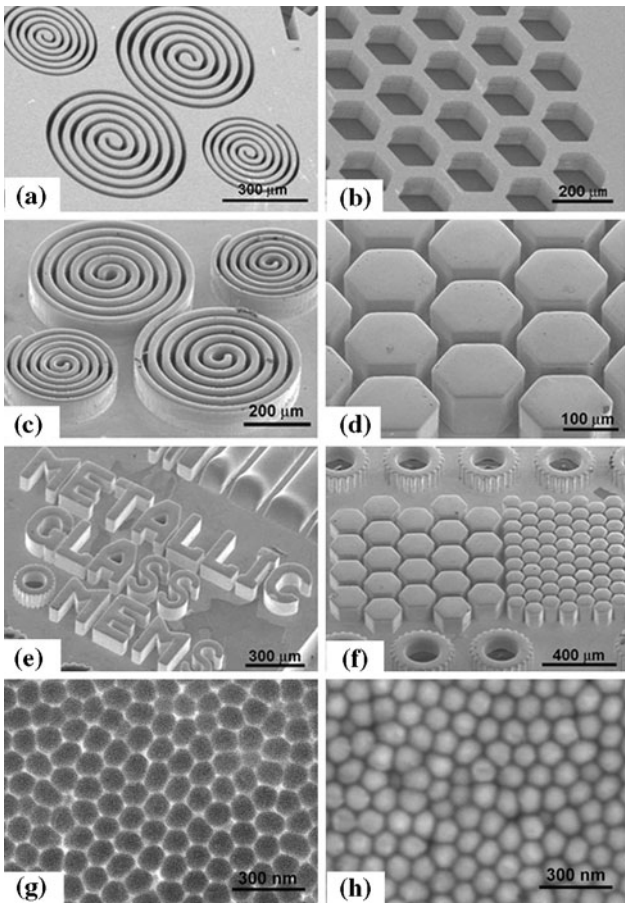

Fig. 4 **a** and **b** are Si molds, **c**–**f** are the patterns fabricated with Si molds, **g** is porous alumina, and **h** is the corresponding nano rods fabricated with the porous alumina **g**. All the above structures are obtained using molding with the $Pd_{40}Ni_{40}Si_4P_{16}$ glassy ribbons

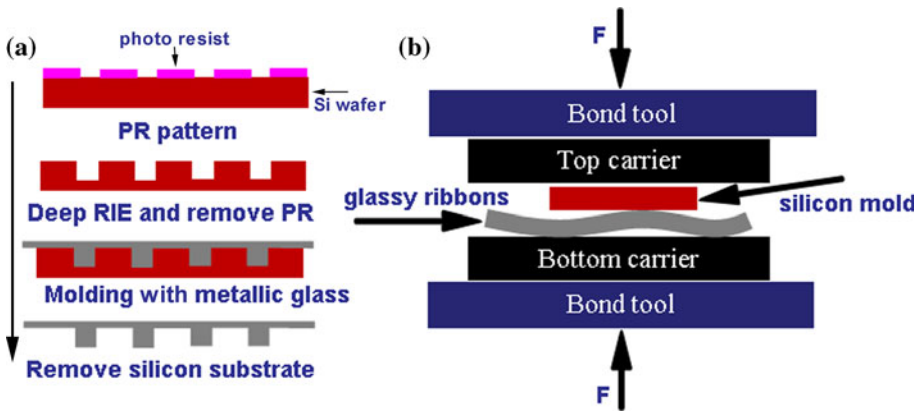

Fig. 3 **a** Steps for molding process with metallic glassy ribbons including the following steps: (1) use photo resist (PR) to pattern Si wafer, (2) use deep reactive ion etch (RIE) to remove the PR and create patterns in Si wafer, (3) mold with metallic glasses, and (4) remove silicon molds. **b** The schematic diagram for thermoplastic forming process

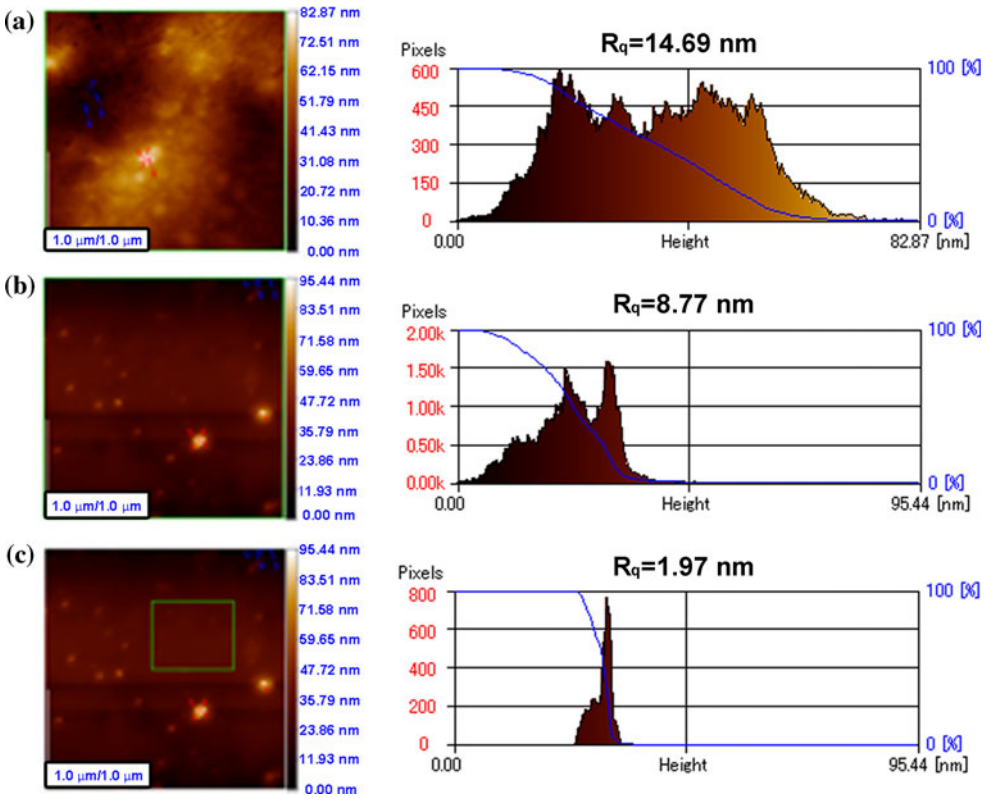

Fig. 5 The root mean square (rms) surface roughness R_q of **a** the original $Pd_{40}Ni_{40}Si_4P_{16}$ glassy ribbons, **b** the ribbons after a replication of a "flat" silicon wafer with roughness of around 1 nm, and **c** the selected region in **b**

(Fig. 5c). So it is suggested that the $Pd_{40}Ni_{40}Si_4P_{16}$ alloy is capable of replicating a minimum feature size of $\sim$2 nm due to the possibility of intrinsically structural inhomogeneity. At the same time, the reproduction of a "flat" surface by TF at the SLR provides a simple approach to prepare flat surfaces for metallic glasses, which can faciliate some property measurements, for example, nanoindentation tests, with critical requirement for surface roughness. Taking advantage of the possibilities of smoothening in the TF region, metallic glasses could be used as the competing materials for micro-mirror devices or components for sliding contact.

Conclusion

Centimeter-scale $Pd_{40}Ni_{40}Si_4P_{16}$ BMGs can be easily fabricated combining fluxing technique and water cooling. The as-cast $Pd_{40}Ni_{40}Si_4P_{16}$ BMGs exhibit a large SLR of 107 K, a high reduced glass transition temperature of 0.596 and a small fragility parameter of 28, demonstrating that this alloy is a good glass former. Taking advantage of the low viscosity and the high thermoplastic formability, the surface of the $Pd_{40}Ni_{40}Si_4P_{16}$ metallic glass can become much smoother by replicating a "flat" Si wafer. This provides an alternative way to create smooth surfaces for metallic glasses.

Acknowledgements We thank Prof. Perepezko at University of Wisconsin-Madison for valuable suggestions and review. We thank Ms. Martin for proofreading. We also appreciate the technical support from Dr. H. Kato. This study is sponsored by "World Premier International Research Center (WPI) Initiative for Atoms, Molecules, and Materials" and partially supported by the Research and Development Project on Advanced Metallic Glasses, Inorganic Materials and Joining Technology and Grant-in-Aid "Priority Area on Science and Technology of Microwave-Induced, Thermally Non-Equilibrium Reaction Field" N: 18070001 from Ministry of Education, Culture, Sports, Science and Technology, Japan.

References

1. Inoue A (1995) Mater Trans, JIM 36:866
2. Greer AL (1995) Science 267:1947
3. Johnson WL (1999) MRS Bull 24:42
4. Inoue A (2000) Acta Mater 48:279
5. Saotome Y, Itoh K, Zhang T, Inoue A (2001) Scr Mater 44:1541
6. Saotome Y, Imai K, Shioda S, Shimizu S, Zhang T, Inoue A (2002) Intermetallics 10:1241
7. Chu JP, Wijaya H, Wu CW, Tsai TR (2007) Appl Phys Lett 90:034101
8. Sharma P, Kaushik N, Kimura H, Saotome Y, Inoue A (2007) Nanotechnology 180:35302
9. Kumar G, Tang HX, Schroers J (2009) Nature 457:868
10. Drehman AJ, Greer AL, Turnbull D (1982) Appl Phys Lett 41:716
11. Kui HW, Greer AL, Turnbull D (1984) Appl Phys Lett 45:615
12. Donovan PE (1989) Acta Metall 37:445
13. Lambson EF, Lambson WA, Macdonald JE, Gibbs MRJ, Saunders GA, Turnbull D (1986) Phys Rev B 33:2380

14. Inoue A, Nishiyama N, Kimura H (1997) Mater Trans, JIM 381:79
15. Chen N, Louzguine-Luzgin DV, Xie GQ, Wada T, Inoue A (2009) Acta Mater 57:2775
16. Chen N, Gu L, Xie GQ, Louzguine-Luzgin DV, Yavari AR, Vaughan G, Perepezko JH, Abe T, Inoue A (2010) Acta Mater 58:5886
17. Chen N, Louzguine-Luzgin DV, Inoue A (2010) Phil Mag Lett 90:771
18. Kissinger HE (1956) J Res Natl Bur Stand 57:217
19. Lu ZP, Liu CT (2002) Acta Mater 50:3501
20. Böhmer R, Nagi KL, Angell CA, Plazek DJ (1993) J Chem Phys 99:4201
21. Angell CA (1985) J Non-Cryst Solids 73:1
22. Angell CA (1995) Science 267:1924
23. Perera DN (1999) J Phys Condens Matter 11:3807
24. Russell KC (1980) Adv Colloid Interface Sci 13:205
25. Herlach DM (1994) Mater Sci Eng R 12:177
26. Xu LM, Buldyrev SV, Giovambattista N, Angell CA, Stanley HE (2009) J Chem Phys 130:054505
27. Hirai N, Eyring H (1958) J Appl Phys 29:810